Momentum dependence of the superconducting gap in $Ba_{1-x}K_xFe_2As_2$

D. V. Evtushinsky,[1] D. S. Inosov,[1,2] V. B. Zabolotnyy,[1] A. Koitzsch,[1] M. Knupfer,[1] B. Büchner,[1] M. S. Viazovska,[3] G. L. Sun,[2] V. Hinkov,[2] A. V. Boris,[2,4] C. T. Lin,[2] B. Keimer,[2] A. Varykhalov,[5] A. A. Kordyuk,[1,6] and S. V. Borisenko[1]

[1]*Institute for Solid State Research, IFW Dresden, P.O. Box 270116, D-01171 Dresden, Germany*

[2]*Max-Planck-Institute for Solid State Research, Heisenbergstrasse 1, D-70569 Stuttgart, Germany*

[3]*Max-Planck-Institute for Mathematics, Vivatsgasse 7, 53111 Bonn, Germany*

[4]*Department of Physics, Loughborough University, Loughborough, LE11 3TU. United Kingdom*

[5]*BESSY GmbH, Albert-Einstein-Strasse 15, 12489 Berlin, Germany*

[6]*Institute of Metal Physics, National Academy of Sciences of Ukraine, 03142 Kyiv, Ukraine*

(Received 24 September 2008; revised manuscript received 30 December 2008; published 17 February 2009)

The precise momentum dependence of the superconducting gap in the iron-arsenide superconductor $Ba_{1-x}K_xFe_2As_2$ (BKFA) with $T_c=32$ K was determined from angle-resolved photoemission spectroscopy (ARPES) via fitting the distribution of the quasiparticle density to a model. The model incorporates finite lifetime and experimental resolution effects, as well as accounts for peculiarities of BKFA electronic structure. We have found that the value of the superconducting gap is practically the same for the inner Γ barrel, X pocket, and "blade" pocket, and equals 9 meV, while the gap on the outer Γ barrel is estimated to be less than 4 meV, resulting in $2\Delta/k_BT_c=6.8$ for the large gap and $2\Delta/k_BT_c<3$ for the small gap. A large $(77\pm3\ \%)$ nonsuperconducting component in the photoemission signal is observed below T_c. Details of gap extraction from ARPES data are discussed in Appendixes A and B.

DOI: 10.1103/PhysRevB.79.054517 PACS number(s): 74.25.Jb, 74.70.−b, 79.60.−i

I. INTRODUCTION

Recently a new class of high-temperature superconductors, iron-based pnictides, attracted much attention due to a rapid increase in the critical temperature, T_c, up to 56 K.[1] These novel materials, still remaining *terra incognita* for theoreticians and experimentalists, require vast efforts from both sides to achieve a progress in the understanding of their nature. One of the most important contributions that experimentalists can make to the development of a theory of any class of superconductors is revealing the magnitude and symmetry of the superconducting gap. Knowledge of the precise momentum dependence of the superconducting gap can provide desirable information about the pairing mechanism that underlies superconductivity in these compounds. Up to now there are a number of papers providing different estimates of the superconducting gap in iron-based superconductors,[2–9] as well as different conclusions about the strength of coupling and applicability of Bardeen-Cooper-Schrieffer (BCS) theory to these compounds. Here we present an angle-resolved photoemission spectroscopy (ARPES) study of the superconducting gap in single crystals of $Ba_{1-x}K_xFe_2As_2$ (BKFA), $T_c=32$ K. The superconducting gap is extracted from photoemission data via a fit to a model that accounts for finite self-energy, temperature, experimental resolution, as well as nonlinearity of the band dispersion, where it is necessary.

II. RESULTS

According to our recent study,[10] the Fermi surface (FS) of BKFA, as seen in ARPES, consists of four different sheets: outer Γ barrel, inner Γ barrel, X pocket, and blade pockets along the XΓ line[11] [see Fig. 1(a)]. X pocket is electronlike, while all other FS sheets are holelike. Figures 1(b) and 1(c) show the same energy-momentum cut [cut1 in Fig. 1(a)] through the distribution of the photoemission intensity at 10 and 45 K, respectively. A backfolding dispersion of the inner Γ barrel develops with cooling below T_c [Figs. 1(b) and 1(c)] that points to the opening of the superconducting gap. To investigate the behavior of the quasiparticle density near the Fermi level (FL) in detail, we plot the symmetrized energy distribution curves (EDC) measured at 10 and 45 K in panels (d) and (e), respectively. The distance between the two peaks in the symmetrized EDC approximately equals to the doubled value of the energy gap, 2Δ. As follows from Figs. 1(d) and 1(e), peaks in EDC, which correspond to the FL crossing of inner Γ barrel, split into two below T_c indicating the opening of a gap of the order of 9 meV, while peaks in the EDC, which refer to the outer Γ barrel, do not split upon cooling, indicating zero (or small in comparison with the peak width) magnitude of the gap on this part of the FS. Figures 1(f) and 1(g) show the energy dependence of the intensity [area under the momentum distribution curve (MDC)], which comes from inner and outer Γ barrels, as extracted from the fit of MDC to four Lorentzians. A pile-up peak clearly develops on the curve that corresponds to the inner Γ barrel, while no such feature is observed for the outer Γ barrel. The resolution-broadened 10 K Fermi cutoff is plotted in panel (g) to show that the difference between 45 and 10 K curves mainly comes from temperature smearing of the Fermi edge. The mentioned arguments allow us to conclude that the inner Γ barrel bears a gap of the order of 9 meV and the gap on the outer one is much smaller.

Although straightforward and unpretentious, "symmetrization" is a rough method for the gap extraction from photoemission data. Therefore below we improve the assessment of the gap magnitude with a robust fitting procedure where the value of the superconducting gap is extracted from the fit of EDC, integrated in a finite momentum window. In this

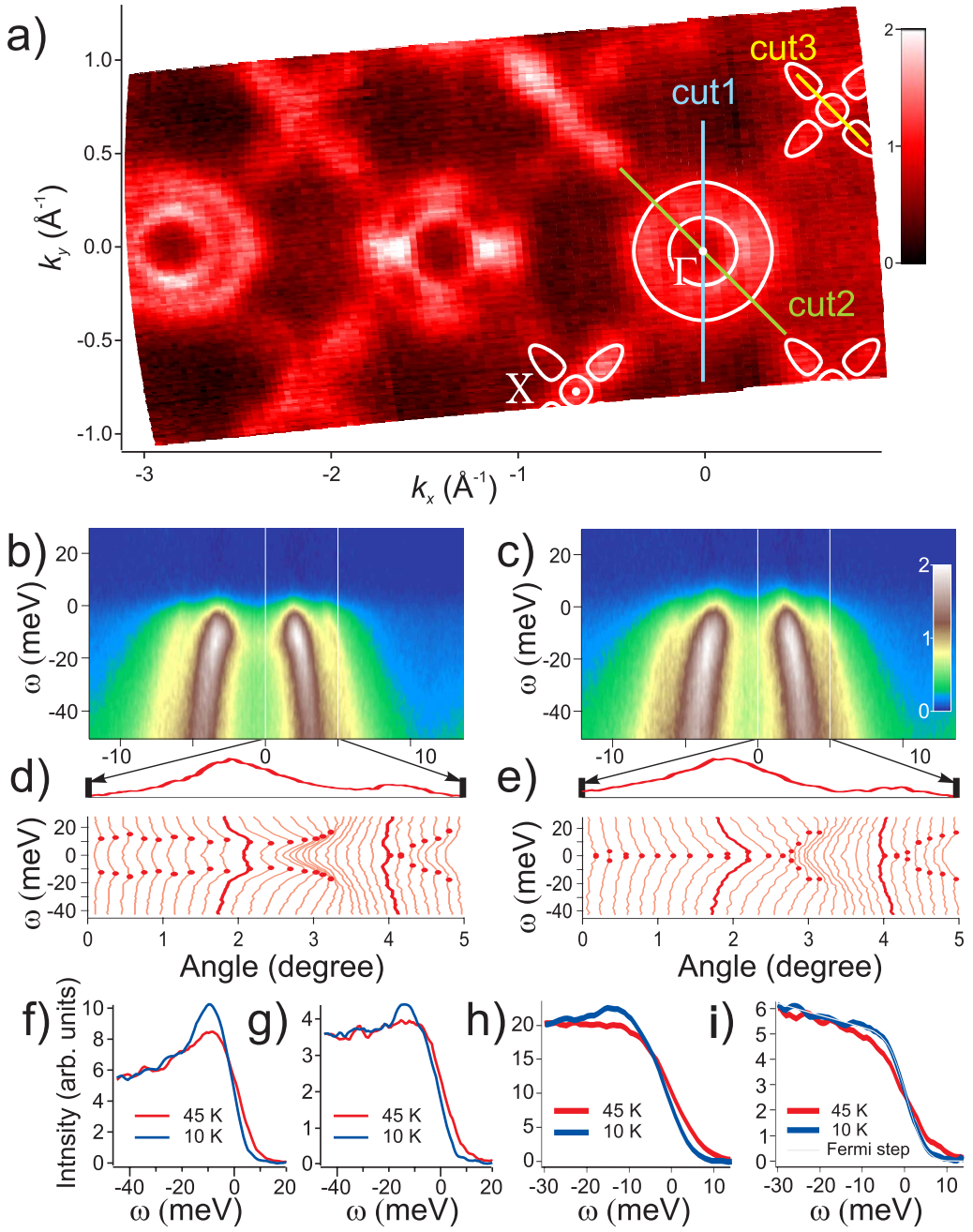

FIG. 1. (Color online) (a) Distribution of the photoemission intensity at the FL with superimposed FS contours (white lines). (b) Momentum-energy cut through the Γ point [cut1 in panel (a)] taken at 10 K. (c) Same cut, taken at 45 K. [(d) and (e)] MDC taken at the FL and symmetrized EDC from cuts (b) and (c), respectively. Maxima of the symmetrized EDC are marked by dots. (f) k_F EDC referring to the inner Γ barrel recorded at 10 and 45 K. (g) Near-k_F EDC emphasizes onset of the superconductivity even better. (h) Energy dependence of the inner Γ-barrel intensity extracted from the fit of MDC. (i) The same for the outer Γ barrel.

case the integration is performed over a very small, compared to the Brillouin-zone size, region, which *does not* imply reduction in momentum-integrated data, and is used only in order to collect the whole available photoemission signal, referring to the particular FL crossing of a single band. The integrated EDC (IEDC) is fitted to the specially derived formula (see Appendix A), which coincides with Dynes function[12] multiplied by the Fermi function and convolved with the response function,

$$\mathrm{IEDC}(\omega) = \left[f(\omega, T) \left| \mathrm{Re} \frac{\omega + i\Sigma''}{E} \right| \right] \otimes R_\omega(\delta E), \qquad (1)$$

where $E = \sqrt{(\omega + i\Sigma'')^2 - \Delta_{\mathbf{k}}^2}$, ω is the binding energy with reversed sign, T is the temperature, Σ'' is the imaginary part of the self-energy, $\Delta_{\mathbf{k}}$ is the momentum-dependent superconducting gap, and δE is the experimental resolution. A similar method of gap extraction is widely used in angle-integrated photoemission spectroscopy.[13] Figure 2(a) shows IEDC that

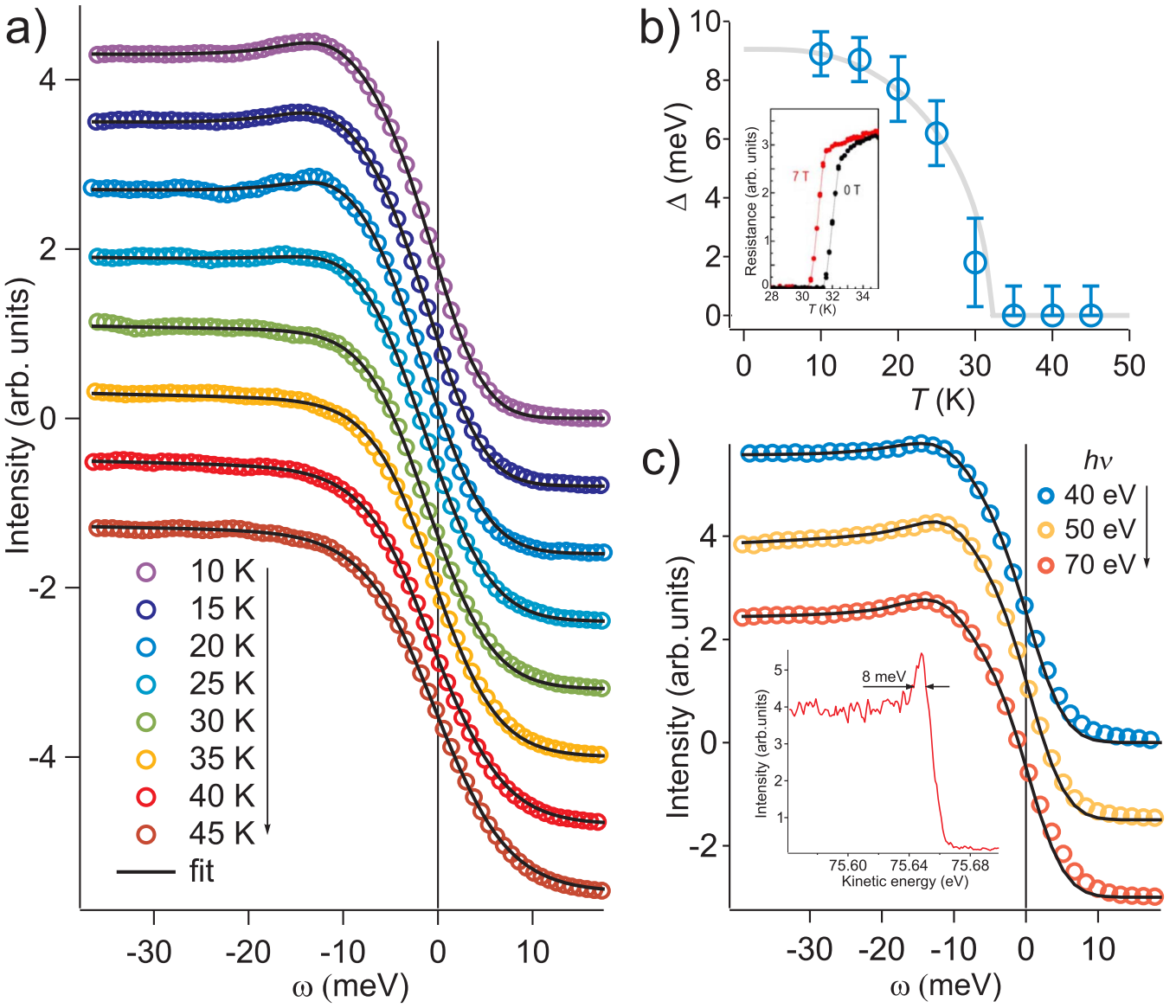

FIG. 2. (Color online) Temperature and momentum dependence of the superconducting gap on the inner Γ barrel. Reliability of the results. (a) Evolution of the integrated EDC from cut1 [see Fig. 1(a)] with temperature and fits to formula (1). EDC are shifted along left axis for clarity. Panel (b) shows the extracted magnitude of the gap plotted against temperature. Inset to (b) shows temperature dependence of resistivity (with and without magnetic field) confirming high quality of the crystals and emphasizing equality of bulk and surface T_c =32 K. (c) Integrated EDC from cut2 [see Fig. 1(a)] measured at different excitation energy at 11 K and corresponding fits to formula (1) reveal reproducibility of the data and robustness of the fitting procedure. EDC are shifted along left axis. The inset in (c) shows a single EDC recorded with $h\nu$=80 eV, demonstrating high resolution at high excitation energies.

refer to the inner Γ barrel, from cut1 [see Fig. 1(a)], measured with 50 eV photon energy at different temperatures, as well as their fits to formula (1). The temperature dependence of the extracted gap shown in Fig. 2(b) illustrates that a superconducting gap develops upon cooling through T_c and reaches the value of 9.1 ± 0.7 meV at low temperatures. Figure 2(c) represents IEDC from cut2 [see Fig. 1(a)] recorded at 11 K with different incident photon energies, $h\nu$. The data exhibit good reproducibility, and the values of the gap extracted for different $h\nu$'s show only a small scattering within the error bars—fit results in 9.4, 9.5, and 10.2 meV for $h\nu$ =40, 50, and 70 eV, respectively. In order to emphasize the quality of our data recorded at high excitation energies, we show a single EDC recorded with $h\nu$=80 eV as an inset to Fig. 2(b). Thus, we can conclude that the momentum anisotropy of the superconducting gap on the inner Γ barrel is absent within 1.5 meV. The outer Γ barrel is much less intense than the neighboring inner Γ barrel, which complicates the analysis. With the same fitting procedure we estimate the gap on the outer Γ barrel to be not more than 4 meV.

Now we turn to the most interesting and problematic region of the BKFA Fermi surface that was not completely resolved in previous studies of iron-arsenic superconductors—a propellerlike structure centered at the X point [see Fig. 1(a)]. Figures 3(a) and 3(b) show the same energy-momentum cut through the X point [cut3 in Fig. 1(a)]

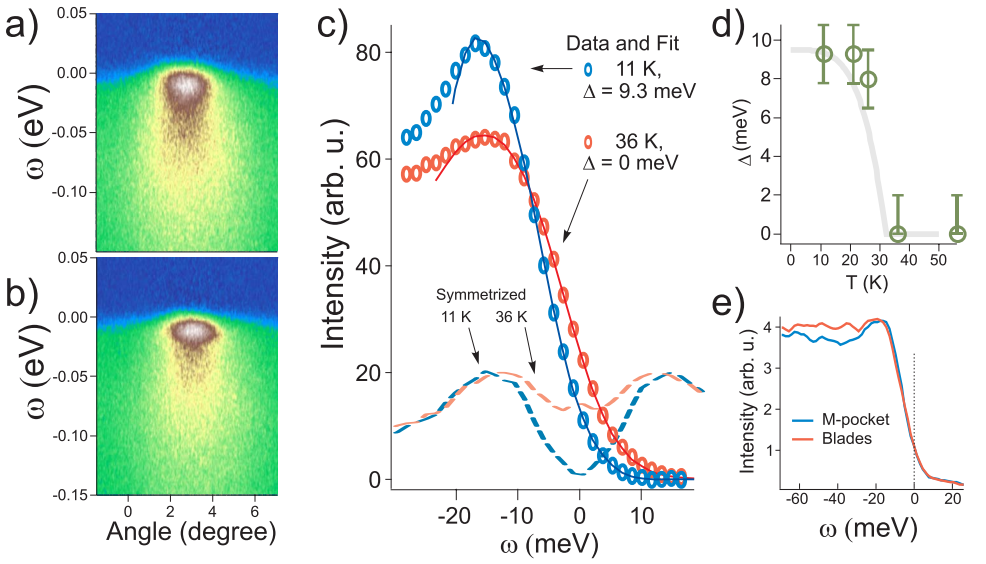

FIG. 3. (Color online) Superconducting gap on the X pocket. (a) Energy-momentum cut through the X point [cut3 on Fig. 1(a)] taken at 36 K. (b) Same cut taken at 11 K. (c) Evolution of the IEDC with temperature and fits to formula (2) and symmetrized k_F EDC. (d) Shows temperature dependence of the gap. (e) Comparison of IEDC referring to the M pocket and to the blades reveals virtually the same values of the superconducting gap.

above (36 K) and below (11 K) T_c, respectively.

Note that the intensity of the blades is largely suppressed for this photon energy and light polarization [see Fig. 1(c) of Ref. 10]. The difficulties with this region in momentum space are related to the presence of the Van Hove singularity close to the FL, which brings the peak in the density of states already above T_c [see Fig. 3(c)]. If both bottom and top of the band are far enough from the FL, then one can treat the dispersion of the band as linear without significant accuracy loss so that formula (1) works well. For the case of band depth comparable to the magnitude of the superconducting gap, formula (1) has to be modified in order to account for the nonlinearity of the normal-state band dispersion. If one assumes that the band possesses electronlike parabolic dispersion with the bottom of the band located at $\omega=-\varepsilon_0$ below the FL, then formula (1) transforms to

$$\mathrm{IEDC}(\omega) = \left[\frac{f(\omega,T)}{2}\left|\mathrm{Re}\left(\frac{\omega+i\Sigma''}{E}\left[\sqrt{\frac{\varepsilon_0}{\varepsilon_0-E}}+\sqrt{\frac{\varepsilon_0}{\varepsilon_0+E}}\right]\right.\right.\right.$$
$$\left.\left.\left.+\sqrt{\frac{\varepsilon_0}{\varepsilon_0-E}}-\sqrt{\frac{\varepsilon_0}{\varepsilon_0+E}}\right)\right|\right]\otimes R_\omega(\delta E). \qquad (2)$$

As it is easy to see, formula (2) reduces to Eq. (1) when ε_0 becomes much larger than ω, Σ'', δE, and $\Delta_{\mathbf{k}}$. For a detailed derivation, see Appendix A.

The depth of the X pocket was determined from the normal-state data using two different methods: a fit of momentum distribution curves taken at different binding energies with two Lorentzians and a fit of the IEDC to formula (2) with $\Delta=0$ and ε_0 as a free parameter. Band depths determined from both methods agree well—the first method results in $\varepsilon_0=20$ meV, while the second one yields $\varepsilon_0=20.5$ meV. Figure 3(c) shows IEDC from cut3 [see Fig. 1(a)], referring to the X pocket, measured at 11 and 36 K, as well as corresponding fits to formula (2). One may note in Fig. 3(c) the leading edge below the Fermi level for high-temperature data, as well as two separate peaks in symmetrized EDC above T_c. These signatures of the gap are not relevant here, as discussed in Appendix B. Temperature dependence of the gap extracted from fitting the data to formula (2) is shown in Fig. 3(d). At low temperatures the gap on the X pocket reaches 9.3 meV. From available experimental data we estimate the gap magnitude on the blades to be also 9 meV [see, e.g., Fig. 3(e)]. The results concerning momentum dependence of the superconducting gap are graphically summarized in Fig. 4. The gap is isotropic within the error bars although, along with similarities to Ref. 4, we see evidence for small anisotropy on the inner Γ barrel—the gap may be slightly larger along ΓX (Brillouin-zone diagonal) than along ΓM (the difference is less than 10%).

Presented analysis of the data via fitting of IEDC allows us to conclude that the low-temperature spectra have superconducting and nonsuperconducting components (see Fig. 5). Only about 23 ± 3 % of the intensity coming from the inner Γ barrel at 10 K refer to the superconducting part of the spectrum.[14] The presence of the two different components in the measured signal can be explained by a phase-separated coexistence of superconducting and normal states, which was already observed in these samples[15] as well as in other similar samples.[16]

III. EXPERIMENTAL DETAILS

Single crystals of BKFA were grown using Sn as flux in a zirconia crucible. The crucible was sealed in a quartz ampoule filled with Ar and loaded into a box furnace. A cooling rate of 3 °C/h was applied from the maximum temperature of 850 down to 550 °C for the growth. The growth details are described in Ref. 17. The crystals were cleaved *in situ* and measured with Scienta SES R4000 analyzer at the base pressure of 5×10^{-11} mbar. ARPES experiments were performed using the "1[3] ARPES" end station at BESSY.

IV. CONCLUSIONS

In conclusion, we proposed a precise procedure for extracting the momentum dependence of the superconducting gap from ARPES spectra. The developed method of data treatment allows us to measure energy gaps with an accuracy

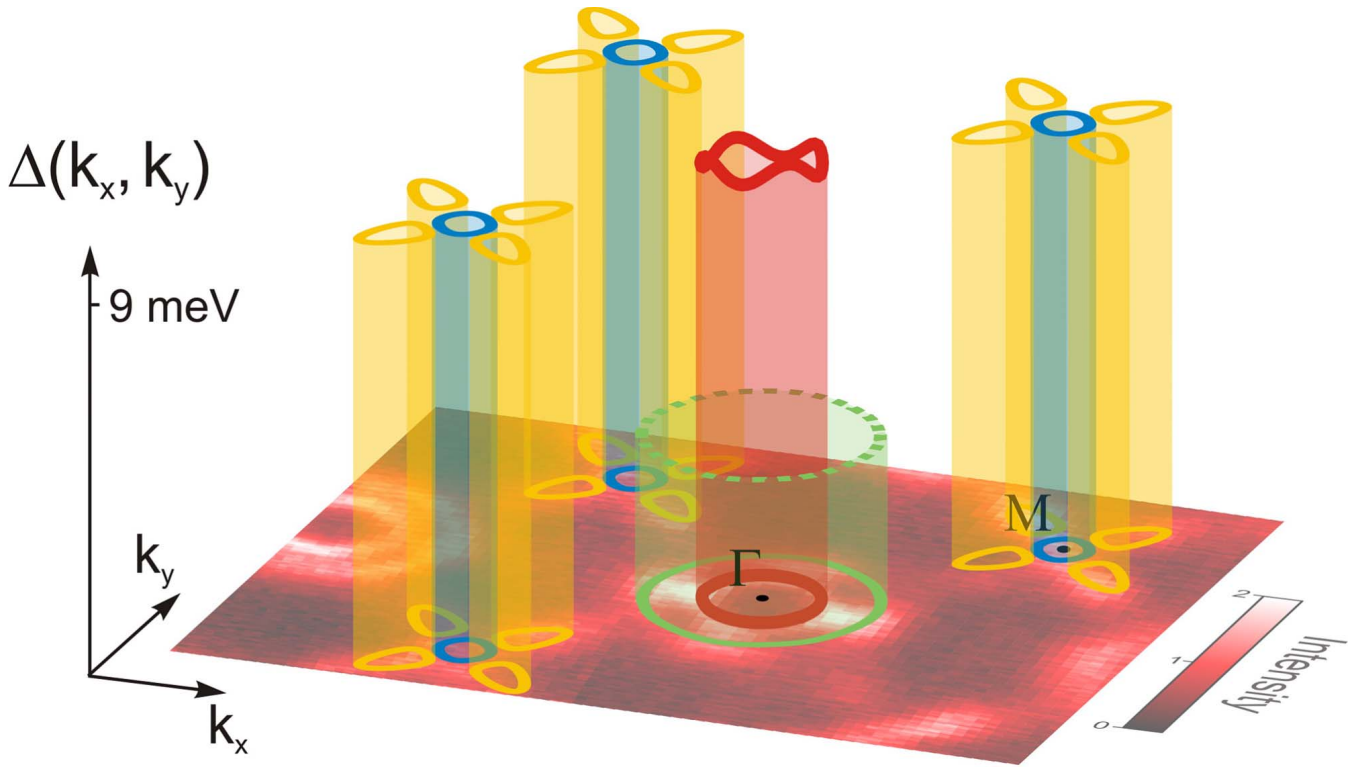

FIG. 4. (Color online) Momentum dependence of the superconducting gap in $Ba_{1-x}K_xFe_2As_2$ (T_c=32 K) is shown as a three-dimensional plot with underlying FS intensity map for orientation. The solid green lines in the basal plane denote the boundaries of the Brillouin zone.

much higher than experimental resolution, similarly to the Voigt-fit procedure,[18] enabling detection of the true values for the MDC width with an accuracy much better than momentum broadening. The IEDC-fitting procedure applied to ARPES spectra of BKFA yielded the following results: (i) the gap on the inner Γ barrel along ΓM equals 9.1 ± 0.7 meV and along ΓX equals 9.7 ± 1 meV; (ii) the gap on the outer Γ barrel is less than 4 meV; (iii) the gap on the X pocket equals 9.3 ± 2 meV; (iv) the gap on the blades is estimated to be 9 meV; (v) at 10 K the imaginary part of the self-energy, Σ″, in the vicinity of the FL was found to be equal to 1–2 meV. Comparison with other ARPES studies of the superconducting gap in iron-based superconductors is shown in Table I. We evaluate the coupling strength as $2\Delta/k_BT_c$=6.8 for the inner Γ barrel, X pocket, and blades, while for the outer Γ barrel $2\Delta/k_BT_c < 3$. A comparison to other experiments is shown in Table II.

Finally, the observation of drastically different superconducting gaps on the inner and outer Γ barrels is in line with theoretically suggested magnetic downfolding[19] and with a hidden (π, π) order observed experimentally.[10] Otherwise it would be hard to expect so different gaps on closely located and very similar bands, formed by slightly different combinations of the same atomic orbitals.

ACKNOWLEDGMENTS

The project was part of the FOR538 and was supported by the DFG under Grants No. KN393/4 and No. BO1912/2-1. We thank I. I. Mazin, A. N. Yaresko, and M. M. Korshunov for useful discussions, as well as R. Hübel, R. Schönfelder, and S. Leger for technical support.

TABLE I. Momentum dependence of the superconducting gap in iron-arsenic superconductors as revealed by ARPES studies sorted by the time of appearance on the arXiv.org. Values of the gap and estimates of the gap anisotropy on the inner Γ barrel are given in meV.

Ref.	2	3	4	5	6	This paper
T_c (K)	53	37	35	53	37	32
Inner Γ barrel	20	12.5	12	15	12	9.2 ± 1
Outer Γ barrel		5.5	8		6	<4
X pocket		(12.5)	(10)		(11)	9 ± 2
Blades			(11)			9 ± 3
Gap anisotropy		<3	2	<5	<3	<1.5

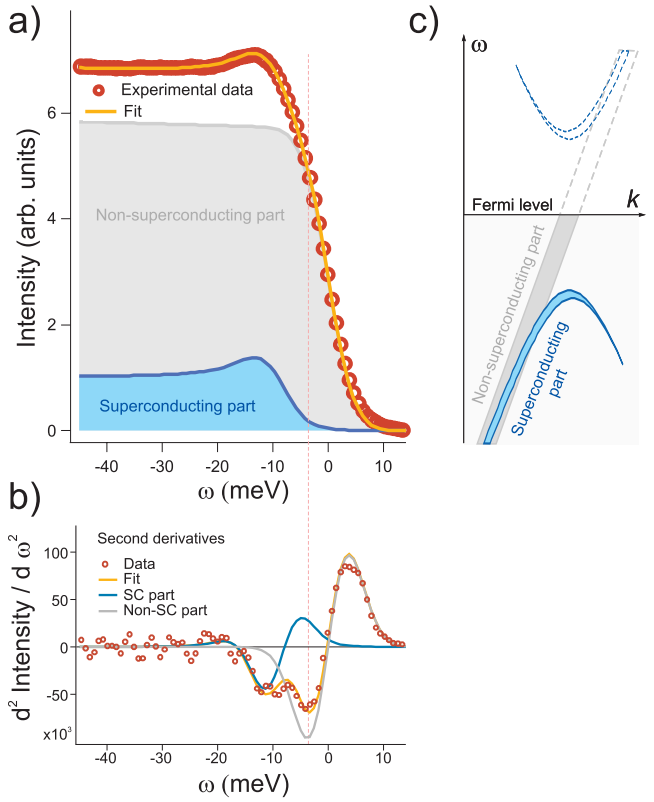

FIG. 5. (Color online) Superconducting and nonsuperconducting constituents of the spectrum. (a) Energy distribution of the intensity corresponding to superconducting and nonsuperconducting parts of the spectrum. (b) Second derivatives of the data and fit. Structure of the second derivative confirms presence of superconducting and nonsuperconducting components. (c) Sketch, illustrating presence of two different components in the same spectrum.

APPENDIX A: FITTING FORMULA

1. Derivation

Below we adduce the detailed derivation of formulas (1) and (2). We also show that for the simple case of negligible curvature of the band dispersion and momentum-independent gap, formula (1) coincides with the Dynes formula.

A very general model for the measured ARPES signal is[20,21]

$$I(k,\omega) = [f(\omega,T)A(k,\omega)] \otimes R_\omega \otimes R_k. \tag{A1}$$

By definition, the integrated EDC is

$$\mathrm{IEDC}(\omega) \equiv \int I(k,\omega)dk. \tag{A2}$$

As soon as we integrate our data over k, momentum resolution does not affect IEDC,[22] which is already an advantage of this method. Substituting Eq. (A1) into Eq. (A2), we get

$$\mathrm{IEDC}(\omega) = \left\{ f(\omega,T)\left[\int A(k,\omega)dk\right]\right\} \otimes R_\omega. \tag{A3}$$

For the spectral function $A(k,\omega)$ in the superconducting state, we use the following well-accepted model:[23]

$$A(k,\omega) = 2\pi[u_k^2\delta(\omega - E_k) + v_k^2\delta(\omega + E_k)], \tag{A4}$$

where

$$u_k^2 = \frac{1}{2}\left(1 + \frac{\xi_k}{E_k}\right), \quad v_k^2 = \frac{1}{2}\left(1 - \frac{\xi_k}{E_k}\right),$$

$$E_k = \sqrt{\xi_k^2 + \Delta^2}. \tag{A5}$$

Substituting Eq. (A4) under the integral into Eq. (A3) and omitting unnecessary constant factors, we get

$$\begin{aligned}\int A(k,\omega_0)dk &= \int [u_k^2\delta(\omega_0 - E_k) + v_k^2\delta(\omega_0 + E_k)]dk \\ &= \frac{1}{2}\left(1 - \frac{\sqrt{\omega_0^2 - \Delta^2}}{\omega_0}\right)\left|\frac{dE_k}{dk}\right|^{-1}\Bigg|_{k=k_1} \\ &\quad + \frac{1}{2}\left(1 + \frac{\sqrt{\omega_0^2 - \Delta^2}}{\omega_0}\right)\left|\frac{dE_k}{dk}\right|^{-1}\Bigg|_{k=k_2},\end{aligned} \tag{A6}$$

where $k_{1,2}$ are solutions of $\xi_{k_{1,2}} = \pm\sqrt{\omega_0^2 - \Delta^2}$. Below we will denote derivative by a prime: $\frac{dE_k}{dk}|_{k=k_1} \equiv E'_{k_1}$.

Expanding the derivative,

$$|E'_k| = \frac{\sqrt{\omega_0^2 - \Delta^2}}{|\omega_0|}|\xi'_k|, \tag{A7}$$

TABLE II. Coupling strength, $2\Delta/k_BT_c$, in iron-arsenic superconductors as revealed by different experimental techniques—compare to the BSC universal value 3.53. Most of the available studies reveal two superconducting gaps of different magnitudes, which are represented in the table as "large" and "small." References 2–6 are ARPES studies, Refs. 7 and 8 are Andreev spectroscopy studies, and Ref. 9 is a specific-heat study.

Ref.	2	3	4	5	6	7	8	9	This paper
Large gap	9	8.1	8.2	6.8	7.5	3.7	9.6	4	6.8
Small gap		3.6	5.5		3.9		3.4		<3

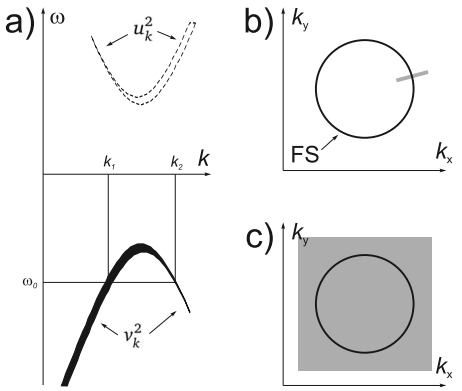

FIG. 6. (a) Spectral function in the superconducting state for the case of linear normal-state dispersion ξ_k. According to formula (A4), the spectral weight above the Fermi level is governed by u_k^2 and by v_k^2 below. (b) Integration in our case is performed along one energy-momentum cut (gray stroke), which intersects Fermi surface at *only one* point. (c) In the momentum-integrated techniques integration is naturally performed over the whole momentum space.

we get

$$\int A(k,\omega_0)dk = \frac{|\omega_0|}{2\sqrt{\omega_0^2-\Delta^2}}[|\xi'_{k_1}|^{-1}+|\xi'_{k_2}|^{-1}] + \frac{1}{2}\mathrm{sgn}(\omega_0)[|\xi'_{k_1}|^{-1}-|\xi'_{k_2}|^{-1}]. \quad \text{(A8)}$$

(In this formula $\xi'_{k_{1,2}}$ implicitly depend on ω_0.)

For the case of the linear band dispersion the derivative is constant, ξ'_k=const, and we arrive at

$$\int A(k,\omega_0)dk = \frac{|\omega_0|}{\sqrt{\omega_0^2-\Delta^2}}. \quad \text{(A9)}$$

This formula coincides with the Dynes function although the premises for the latter are somewhat different, requiring the assumption of the momentum-independent gap. Important difference in definition of our IEDC and the well-known Dynes function is that the former is a trace integral along one direction [see Fig. 6(b)], while the latter is a double integral over the whole momentum space [see Fig. 6(c)],

$$\mathrm{dyn}(\omega) \equiv \int\int A(\mathbf{k},\omega)dk_x dk_y. \quad \text{(A10)}$$

Substituting here the aforementioned model for spectral function (A4), we go from a double integral to the integration along the contour,

$$\mathrm{dyn}(\omega_0) = \oint_{\mathbf{k}:\xi_\mathbf{k}=\sqrt{\omega_0^2-\Delta^2}} v_\mathbf{k}^2|\nabla E_\mathbf{k}|^{-1}dk + \oint_{\mathbf{k}:\xi_\mathbf{k}=-\sqrt{\omega_0^2-\Delta^2}} v_\mathbf{k}^2|\nabla E_\mathbf{k}|^{-1}dk. \quad \text{(A11)}$$

When the depth of the band is much larger than the value of the superconducting gap, i.e., when we can neglect the nonlinearity of the dispersion (which is an important condition for the Dynes formula to hold), this expression reduces to the integral over the Fermi surface,

$$\mathrm{dyn}(\omega_0) = \oint_{\mathbf{k}:\xi_\mathbf{k}=0} |\nabla E_\mathbf{k}|^{-1}dk. \quad \text{(A12)}$$

Here we expand $\nabla E_\mathbf{k}$ similarly to formula (A7), and get

$$\mathrm{dyn}(\omega_0) = \oint_{\mathbf{k}:\xi_\mathbf{k}=0} \frac{|\omega_0|}{\sqrt{\omega_0^2-\Delta^2}}|\nabla \xi_\mathbf{k}|^{-1}dk. \quad \text{(A13)}$$

As soon as ω_0 and Δ (in this case) do not depend on $\mathbf{k}$, one can pull them out from under the integral,

$$\mathrm{dyn}(\omega_0) = \frac{|\omega_0|}{\sqrt{\omega_0^2-\Delta^2}}\oint_{\mathbf{k}:\xi_\mathbf{k}=0} |\nabla \xi_\mathbf{k}|^{-1}dk. \quad \text{(A14)}$$

The integrand does not depend on ω_0, therefore the whole integral is unnecessary for our purposes constant factor, which can be omitted, and we arrive at the same result as Eq. (A9),

$$\mathrm{dyn}(\omega_0) = \frac{|\omega_0|}{\sqrt{\omega_0^2-\Delta^2}}. \quad \text{(A15)}$$

2. Finite lifetime

Up to now we have the result [formula (A8)] obtained under the assumption of infinitely large lifetime or, in other words, for very sharp bands. In such a case in order to get the formula that incorporates effects of the finite lifetime, the following recipe is often used: take the formula, derived for infinite lifetime, add to the argument the imaginary part, and take the real part of the result,

$$g(\omega) \to \mathrm{Re}\, g(\omega + i\Sigma''). \quad \text{(A16)}$$

Below we show that in our case this trick provides the exact result.

In order to account for lifetime broadening rigorously, one has to substitute a Lorentzian in Eq. (A4) for the delta function,

$$\delta(\omega-E_k) \to L^{\Sigma''}(\omega-E_k) = \frac{1}{2\pi}\frac{\Sigma''}{(\omega-E_k)^2+\Sigma''^2},$$

which results in the possibility to rewrite the expression for the spectral function in the following way:

$$A^{\Sigma''}(k,\omega) = A(k,\omega) \otimes L^{\Sigma''}(\omega-E_k), \quad \text{(A17)}$$

where $A(k,\omega)$ stands for nonbroadened spectral function (A4). As convolution over ω commutes with integration over k,

$$\int A^{\Sigma''}(k,\omega)dk = \left[\int A(k,\omega)dk\right] \otimes L^{\Sigma''}. \tag{A18}$$

We already know the result for integration of the spectral function over momentum [formula (A8)], and now the only problem is to evaluate the convolution. We will do it for linear and quadratic band dispersions, i.e., input parameters to derive formulas (1) and (2).

Let $g(\omega) \equiv \int A(k,\omega)dk$, then in order to evaluate the convolution in Eq. (A18), we have to calculate the integral $\int_{-\infty}^{+\infty} g(\omega) L^{\Sigma''}(\omega_0 - \omega)d\omega$.

The function $g(\omega)$ is defined on the real axis. Once we know the analytic function $\tilde{g}(z)$, $z \in \mathbb{C}$, such that $\mathrm{Re}[\tilde{g}(\omega)] = g(\omega)$ for $\omega \in \mathbb{R}$, we can calculate the required integral with the help of Cauchy's residue theorem,

$$\begin{aligned}
&\int_{+\infty}^{-\infty} g(\omega) L^{\Sigma''}(\omega_0 - \omega)d\omega \\
&= \mathrm{Re}\left[\int_{+\infty}^{-\infty} \tilde{g}(\omega) L^{\Sigma''}(\omega_0 - \omega)d\omega\right] \\
&= \mathrm{Re}\left[\lim_{R\to\infty,\ \eta\to 0} \oint_{\Gamma_{R,\eta}} \tilde{g}(z) L^{\Sigma''}(\omega_0 - z)dz\right] \\
&= \wr\, \tilde{g} \text{ possesses no poles inside } \Gamma_{R,\eta} \wr \\
&= \mathrm{Re}\left[2\pi i \operatorname*{Res}_{z=\omega_0+i\Sigma''} \tilde{g}(z) \frac{1}{2\pi} \frac{\Sigma''}{(\omega_0 - z)^2 + \Sigma''^2}\right] \\
&= \mathrm{Re}[\tilde{g}(\omega_0 + i\Sigma'')],
\end{aligned} \tag{A19}$$

which coincides with formula (A16) and implies formulas (1) and (2) as corollaries. For definition of the integration contour $\Gamma_{R,\eta}$ refer to Fig. 7. Explicit form of the function $\tilde{g}(z)$ for linear band dispersion is

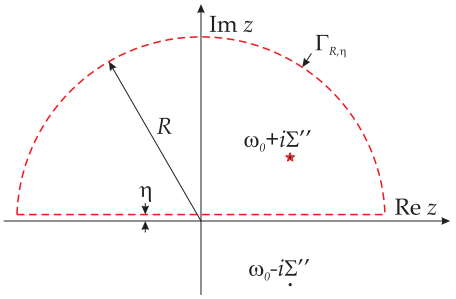

FIG. 7. (Color online) Integration along the contour on the complex plane. According to Cauchy's residue theorem, the integral along the contour $\Gamma_{R,\eta}$ equals to the residue in the pole of the integrand inside, $\omega_0 + i\Sigma''$.

$$\tilde{g}_1(z) = \frac{z}{\sqrt[*]{z^2 - \Delta^2}}, \tag{A20}$$

where for $z = re^{i\phi}$ we pick the following definition of the square root $\sqrt[*]{z} \equiv r^{1/2} e^{i\phi/2}$, $\phi \in [0, 2\pi)$.

For quadratic dispersion we get

$$\tilde{g}_2(z) = \frac{1}{2} \frac{z}{\sqrt[*]{z^2 - \Delta^2}} \left(\frac{1}{k_1} + \frac{1}{k_2}\right) + \frac{1}{2}\left(\frac{1}{k_1} - \frac{1}{k_2}\right), \tag{A21}$$

where $k_{1,2} = \sqrt[**]{\varepsilon_0 \pm \sqrt[*]{z^2 - \Delta^2}}$, $\sqrt[**]{z} \equiv r^{1/2} e^{i\phi/2}$, $\phi \in [-\pi, \pi)$.

Defined in such a way, $\tilde{g}_{1,2}(z)$ are analytic in $\mathbb{C} \backslash (-\infty, +\infty)$, i.e., all conditions for Cauchy's residue theorem are fulfilled.

3. Formulas in real numbers

For numerical calculations it is useful to rewrite formula (1) without the use of complex numbers:

$$\mathrm{IEDC}(\omega) = \left[f(\omega,T) \left| \frac{\omega(a+c) + \Sigma''b}{\sqrt{2}c\sqrt{a+c}} \right| \right] \otimes R_\omega(\delta E), \tag{A22}$$

where $a = \omega^2 - \Sigma''^2 - \Delta_{\mathbf{k}}^2$, $b = 2\Sigma''\omega$, and $c = \sqrt{a^2 + b^2}$.

Similarly, formula (2) can be rewritten as

$$\begin{aligned}
\mathrm{IEDC}(\omega) = \Bigg[f(\omega,T) \frac{1}{2} \sqrt{\varepsilon_0} \Bigg(& \frac{|\omega[(a+c)(\alpha_1+\gamma_1) + b\beta_1] + \Sigma''[b(\alpha_1+\gamma_1) - \beta_1(a+c)]|}{2c\gamma_1\sqrt{a+c}\sqrt{\alpha_1+\gamma_1}} \\
& + \frac{|\omega[(a+c)(\alpha_2+\gamma_2) + b\beta_2] + \Sigma''[b(\alpha_2+\gamma_2) - \beta_2(a+c)]|}{2c\gamma_2\sqrt{a+c}\sqrt{\alpha_2+\gamma_2}} - \mathrm{sgn}(\omega) \left[\frac{\sqrt{\alpha_1+\gamma_1}}{\sqrt{2}\gamma_1} - \frac{\sqrt{\alpha_2+\gamma_2}}{\sqrt{2}\gamma_2}\right] \Bigg) \Bigg] \otimes R_\omega(\delta E),
\end{aligned} \tag{A23}$$

where

$$a = \omega^2 - \Sigma''^2 - \Delta_{\mathbf{k}}^2, \quad b = 2\Sigma''\omega, \quad c = \sqrt{a^2 + b^2},$$

$$\alpha_{1,2} = \varepsilon_0 \mp \sqrt{\frac{a+c}{2}}, \quad \beta_{1,2} = \pm \frac{b}{\sqrt{2}\sqrt{a+c}},$$

$$\text{and} \quad \gamma_{1,2} = \sqrt{\alpha_{1,2}^2 + \beta_{1,2}^2}.$$

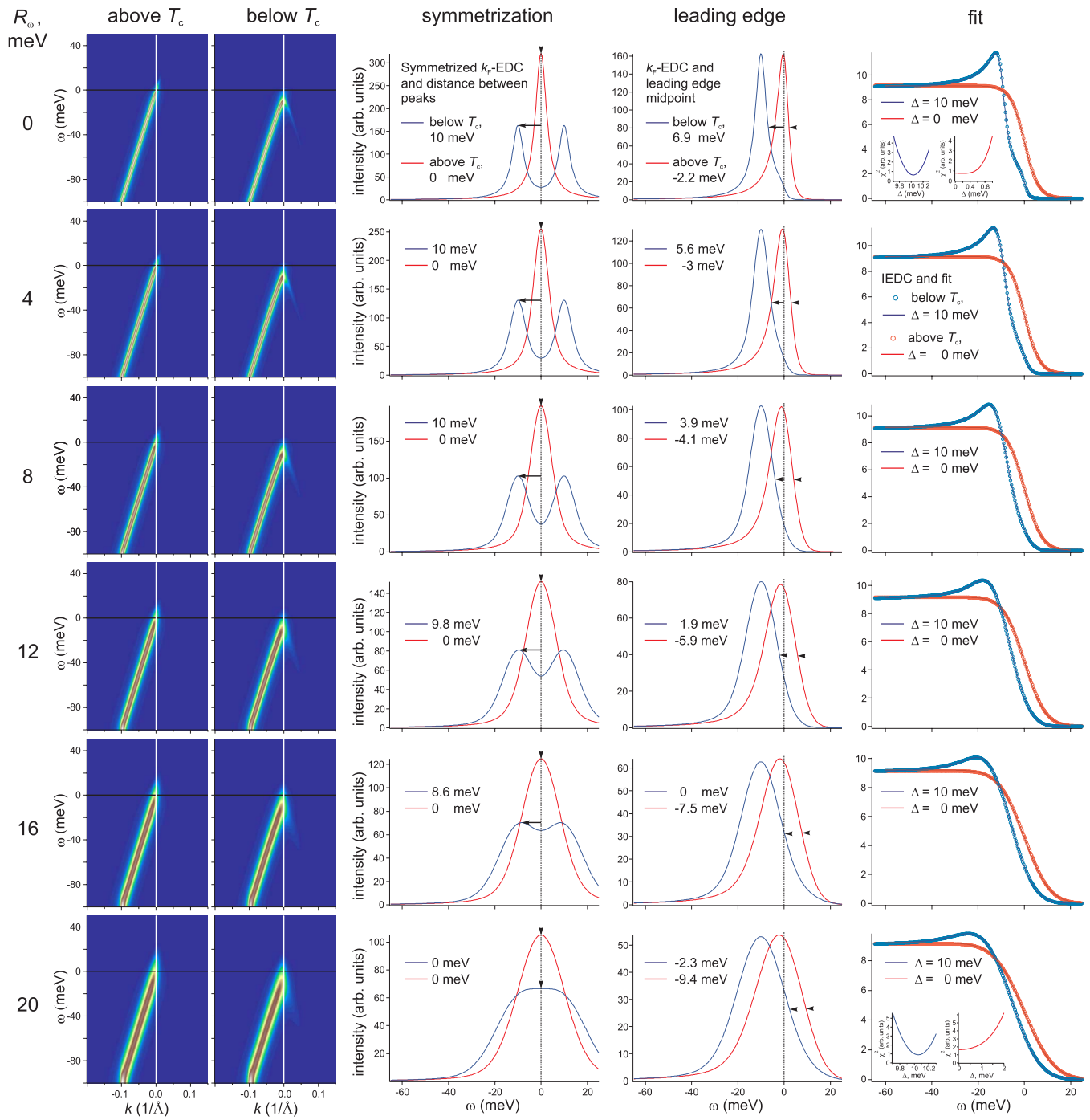

FIG. 8. (Color online) Influence of the energy resolution on the determination of the gap via symmetrization, leading edge, and fit. First column: energy resolution for the corresponding row. Second column: simulated energy-momentum cut above T_c ($\Sigma''=3$ meV, $kT=3$ meV, and $\Delta=0$ meV). Third column: simulated energy-momentum cut below T_c ($\Sigma''=3$ meV, $kT=1$ meV, and $\Delta=10$ meV). Fourth column: determination of the gap with symmetrization. Fifth column: determination of the gap with leading edge. Sixth column: determination of the gap with fit to formula (1) and χ^2 criterion as insets to some panels. Symmetrization and leading edge provide acceptable results for good resolution and fail when the resolution becomes worse. The fitting procedure always provides the correct result.

APPENDIX B: EXTRACTION OF THE GAP FROM THE MODELED DATA BY SYMMETRIZATION, LEADING EDGE, AND FITTING

The symmetrization is highly valued by some part of the ARPES community. We strongly believe that symmetrization is to be substituted by more rigorous and advanced ways of data treatment, such as those used in very recent publications on photoemission spectroscopy of superconductors.[24,25]

Below we model ARPES spectra with formulas (A1) and (A2), extract the gap with symmetrization and leading edge,[20] and proposed here fit of the IEDC. Results confirm that the fitting procedure is robust against momentum reso-

TABLE III. Superconducting gap as extracted from modeled data (Fig. 8) with different methods. All numbers are given in meV. The correct value of the gap (implemented in simulation) equals 10 meV.

R_ω	Symmetrization	Leading edge shift	Fit
0	10	9.1	10 ± 0.1
4	10	8.6	10
8	10	8.0	10
12	9.8	7.8	10
16	8.6	7.5	10
20	0	7.1	10 ± 0.1

lution, properly accounts for energy resolution and finite lifetime, provides correct values even in the case of the nonlinear band dispersion, and allows one to disentangle nonsuperconducting and superconducting parts of the spectrum. At the same time, symmetrization and leading edge are not stable with respect to the effects of the experimental resolution and, furthermore, fail in the case of the shallow band and in the presence of the nonsuperconducting component.

1. Energy resolution

First, we study the influence of the experimental energy resolution on the determination of the gap from ARPES data with symmetrization, leading edge, and fit to formula (1) from the paper. The results of these studies are shown in Fig. 8 and summarized in Table III. Please note that *not* the resolution of the analyzer is important but the resolution of the *whole* photoemission experiment. Also it is worthwhile to mention that effects of the lifetime broadening are in some respect similar to the effects of energy resolution as they both lead to the broadening of the spectra.

By the way, leading edge (the lowest binding energy at which the k_F EDC reaches half of its maximum) alone is not a good measure of the gap (see corresponding columns in Figs. 8–10), while leading edge shift (shift of the leading edge with respect to the position in the normal state) is a lot more relevant quantity.

2. Momentum resolution

Next, we consider the influence of the experimental momentum resolution on the determination of the gap from ARPES data with symmetrization, leading edge, and the fitting to formula (1). The results of these studies are shown in Fig. 9 and summarized in Table IV. Note that not the resolution of the analyzer is important but the resolution of the whole photoemission experiment.

The width (full width at half maximum) of the narrowest EDC from Refs. 2–6, as well as from our studies, is 8–10 meV. The momentum resolution is about 0.1 Å^{-1}.

3. Nonlinearity of the band dispersion

The case when the band depth is comparable to the value of the superconducting gap is quite complicated and really requires special treatment. That is why formula (2) has been derived and used to fit the data. It is easy to mistake the Van Hove singularity for the gap when using simplified methods of data analysis. Masking effects of Van Hove singularity is one of the real examples where symmetrization and leading edge give wrong results (Fig. 10 and especially column three bottom row). Naturally, such "gap" will not close at T_c.

Here we have modeled the influence of the nonlinearity of the band dispersion in conjunction with experimental momentum resolution on the determination of the gap from ARPES data with symmetrization, leading edge, and fit to formula (2). The results of these studies are shown in Fig. 10 and summarized in Table V.

TABLE IV. Superconducting gap as extracted from modeled data (Fig. 9) with different methods. All numbers, except for momentum resolution, are given in meV. The correct value of the gap (implemented in simulation) equals 10 meV. Parameters $R_\omega = 10$ meV and $R_k = 0.1$ Å^{-1} correspond to the experimentally observed widths of the spectra.

R_ω	R_k (10^{-3} Å^{-1})	Symmetrization	Leading edge shift	Fit
0	0	10.0	9.1	10
0	50	12.0	8.2	10
0	100	12.3	8.0	10
0	200	12.4	7.5	10
10	100	16	6.4	10
20	200	23	4.9	10 ± 0.5

4. Nonsuperconducting component

According to recent μSR (muon spin rotation) studies, superconducting fraction for optimally doped BKFA samples (those used in Refs. 2–6) comprises 50% of the sample volume (see Ref. 16), and for our slightly underdoped samples it comprises only 25% (see Ref. 15). Under these circumstances, the leading edge is completely irrelevant to the gap value while symmetrization may provide some estimates of the value of the gap depending on other conditions (resolution, lifetime, etc.). Fitting in this case is indispensable as it

TABLE V. Superconducting gap, as extracted from modeled data (Fig. 10) with different methods. All numbers, except for momentum resolution, are given in meV.

R_k (10^{-3} Å^{-1})	Input to the model	Symmetrization	Leading edge	Fit
0	0	0	−1.9	0+0.8
	10	10.1	6.9	10 ± 0.1
45	0	10.9	0.5	0+0.8
	10	12.4	7.9	10 ± 0.1
60	0	18	3.5	0+0.8
	10	20	8.3	10 ± 0.1

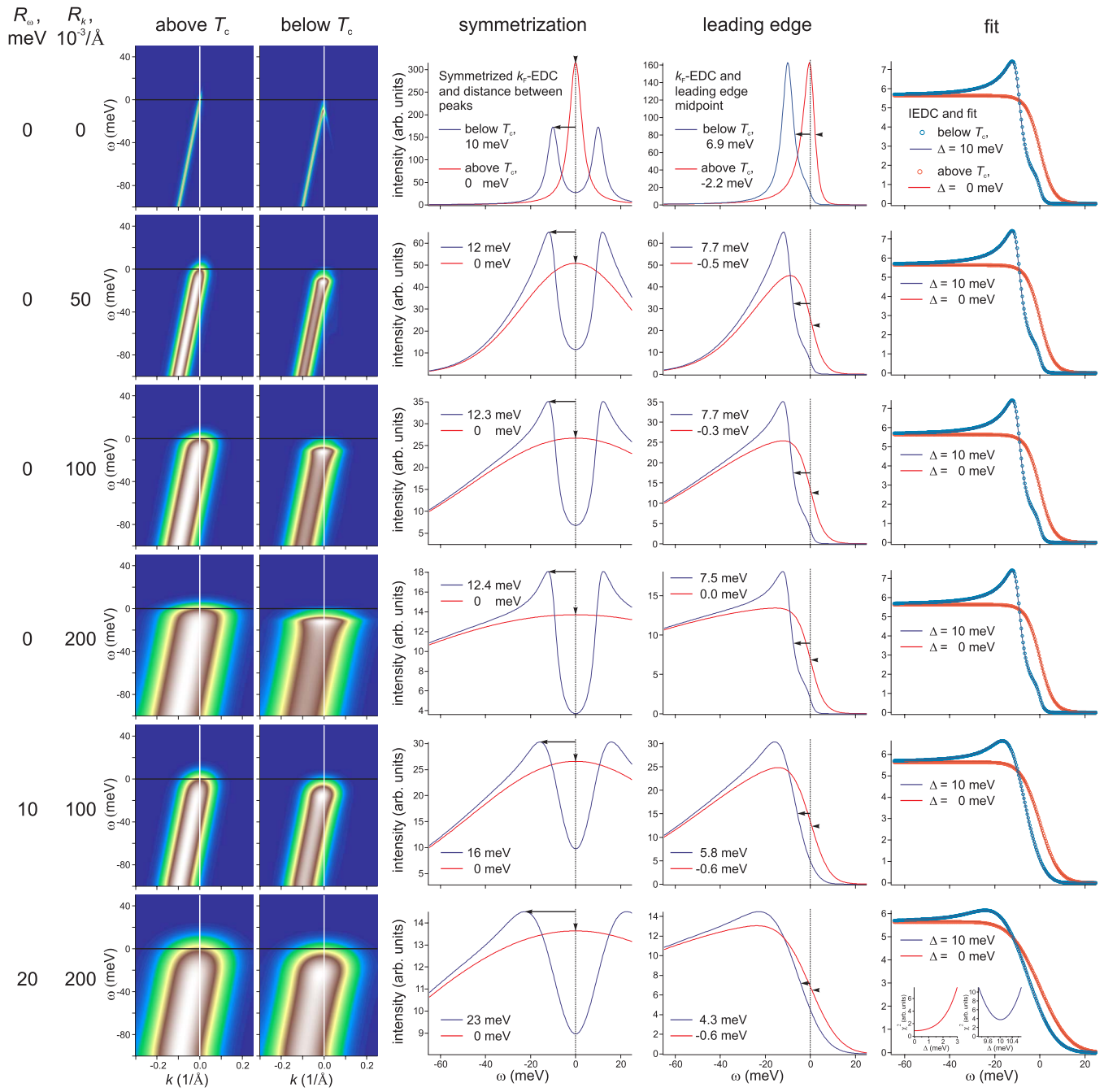

FIG. 9. (Color online) Influence of the momentum resolution on the determination of the gap via symmetrization, leading edge, and fit. First column: energy resolution for the corresponding row. Second column: momentum resolution for the corresponding row. Third column: simulated energy-momentum cut above T_c ($\Sigma''=3$ meV, $kT=3$ meV, and $\Delta=0$ meV). Fourth column: simulated energy-momentum cut below T_c ($\Sigma''=3$ meV, $kT=1$ meV, and $\Delta=10$ meV). Fifth column: determination of the gap with symmetrization. Sixth column: determination of the gap with leading edge. Seventh column: determination of the gap with fit to formula (1) and χ^2 criterion as insets to some panels. Symmetrization and leading edge provide acceptable results for good resolution and fail when the resolution becomes worse. The fitting procedure always provides the correct result.

not only reveals precise values of the gap but also allows us to determine the fractions of the superconducting and nonsuperconducting signals (see Fig. 5). For our crystals these fractions determined from two completely different methods—μSR and the fit of the ARPES data—perfectly match each other.

5. Renormalization

Presence of the dispersion anomalies, "kinks," can affect position of the leading edge and peaks in the symmetrized EDC and can be mistaken for energy gap, similarly to the discussed above Van Hove singularity. In the case of linear

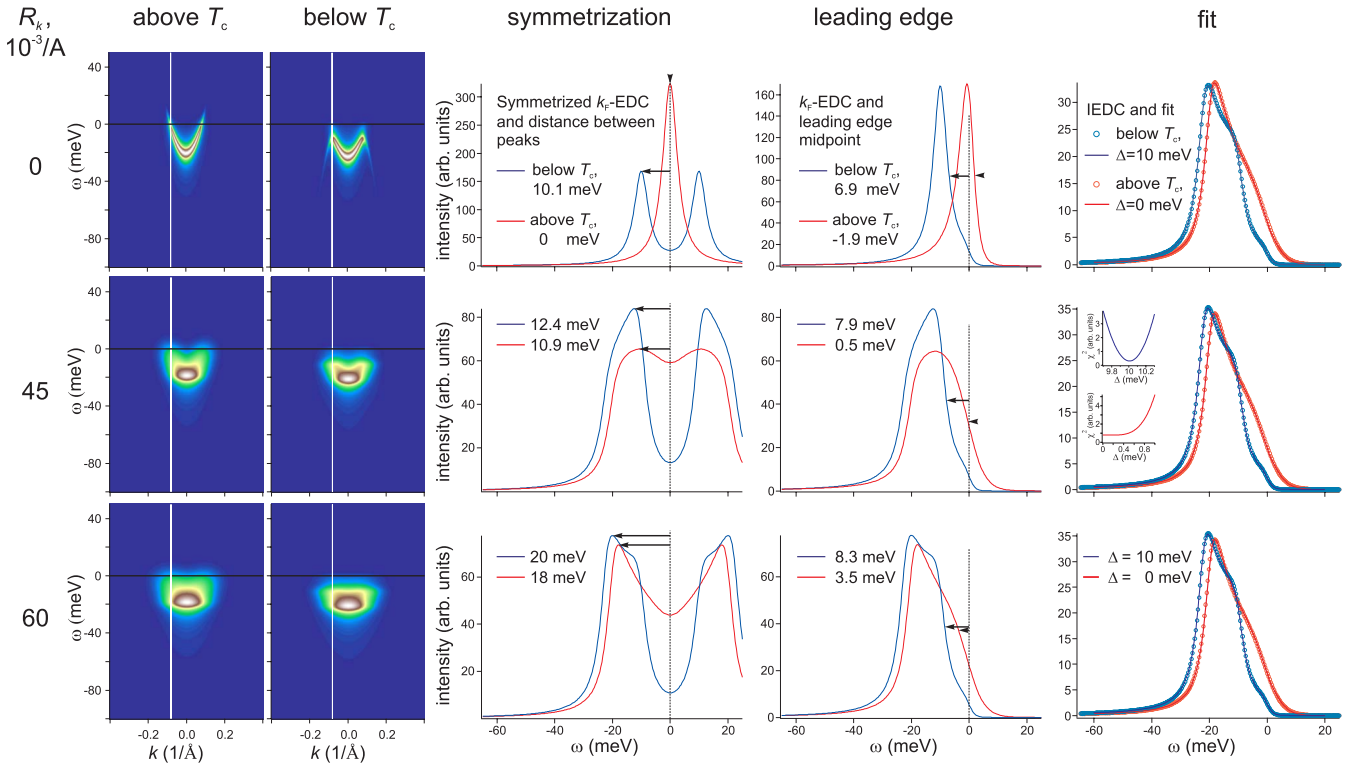

FIG. 10. (Color online) Influence of the small band depth on the determination of the gap via symmetrization, leading edge, and fit. First column: momentum resolution for the corresponding row. Second column: simulated energy-momentum cut above T_c ($\Sigma''=3$ meV, $kT=3$ meV, $\Delta=0$ meV, and $\varepsilon_0=20$ meV). Third column: simulated energy-momentum cut below T_c ($\Sigma''=3$ meV, $kT=1$ meV, $\Delta=10$ meV, and $\varepsilon_0=20$ meV). Fourth column: determination of the gap with symmetrization. Fifth column: determination of the gap with leading edge. Sixth column: determination of the gap with fit to formula (2) and χ^2 criterion as insets to some panels. First row: no resolution effects added. Second row: small resolution effects are added. Third row: moderate resolution effects are added (resolution effects are comparable and may be even smaller to those in the real data, which is easy to see comparing these energy-momentum cuts to those directly measured). For simplicity, only momentum resolution is added. Symmetrization and leading edge provide acceptable results for good resolution and fail when the resolution becomes worse. The fitting procedure always provides the correct result.

bare band dispersion,[26] IEDC is not affected by self-energy at all,

$$\int_{-\infty}^{+\infty} \frac{1}{2\pi} \frac{\Sigma''(\omega)}{(\omega - \Sigma'(\omega) - v_F k)^2 + \Sigma''(\omega)^2} dk = \frac{1}{v_F}. \quad \text{(B1)}$$

6. Summary

(1) The proposed fitting procedure is a rigorous and precise method of gap extraction, which accounts for several important features of $Ba_{1-x}K_xFe_2As_2$ photoemission spectra: (a) nonlinearity of the band dispersion; (b) presence of large nonsuperconducting component; and (c) experimental resolution.

(2) Symmetrization is not a universal way for the extraction of the gap from spectroscopic data since it is highly sensitive to experimental resolution and nonlinearity of the band dispersion. For example, it (a) gives zero value for the gap while there is substantial gap (Fig. 8, bottom row) and (b) gives substantial value for the gap, while actual gap is zero (Fig. 10, bottom row).

(3) Leading edge alone is not a good measure of the gap (see bottom rows of Figs. 8–10), while leading edge shift in the absence of the nonsuperconducting component is quite good although still a rough measure of the gap and provides result with an accuracy better than 50% even under severe conditions (see Tables III–V).

[1] C. Wang, L. Li, S. Chi, Z. Zhu, Z. Ren, Y. Li, Y. Wang, X. Lin, Y. Luo, S. Jiang, X. Xu, G. Cao, and X. Zhu'an, EPL **83**, 67006 (2008).

[2] C. Liu, T. Kondo, M. E. Tillman, R. Gordon, G. D. Samolyuk, Y. Lee, C. Martin, J. L. McChesney, S. Bud'ko, M. A. Tanatar, E. Rotenberg, P. C. Canfield, R. Prozorov, B. N. Harmon, and A. Kaminski, arXiv:0806.2147 (unpublished).

[3] H. Ding, P. Richard, K. Nakayama, K. Sugawara, T. Arakane, Y. Sekiba, A. Takayama, S. Souma, T. Sato, T. Takahashi, Z. Wang, X. Dai, Z. Fang, G. F. Chen, J. L. Luo, and N. L. Wang, EPL **83**,

47001 (2008).
[4] L. Zhao, H. Liu, W. Zhang, J. Meng, X. Jia, G. Liu, X. Dong, G. F. Chen, J. L. Luo, N. L. Wang, W. Lu, G. Wang, Y. Zhou, Y. Zhu, X. Wang, Z. Zhao, Z. Xu, C. Chen, and X. J. Zhou, Chin. Phys. Lett. **25**, 4402 (2008).
[5] T. Kondo, A. F. Santander-Syro, O. Copie, Chang Liu, M. E. Tillman, E. D. Mun, J. Schmalian, S. L. Bud'ko, M. A. Tanatar, P. C. Canfield, and A. Kaminski, Phys. Rev. Lett. **101**, 147003 (2008).
[6] L. Wray, D. Qian, D. Hsieh, Y. Xia, L. Li, J. G. Checkelsky, A. Pasupathy, K. K. Gomes, A. V. Fedorov, G. F. Chen, J. L. Luo, A. Yazdani, N. P. Ong, N. L. Wang, and M. Z. Hasan, arXiv:0808.2185 (unpublished).
[7] T. Y. Chen, Z. Tesanovic, R. H. Liu, X. H. Chen, and C. L. Chien, Nature (London) **453**, 1224 (2008).
[8] P. Szabo, Z. Pribulova, G. Pristas, S. L. Bud'ko, P. C. Canfield, and P. Samuely, arXiv:0809.1566 (unpublished).
[9] G. Mu, H. Luo, Z. Wang, L. Shan, C. Ren, and H.-H. Wen, arXiv:0808.2941 (unpublished).
[10] V. B. Zabolotnyy, D. S. Inosov, D. V. Evtushinsky, A. Koitzsch, A. A. Kordyuk, J. T. Park, D. Haug, V. Hinkov, A. V. Boris, D. L. Sun, G. L. Sun, C. T. Lin, B. Buechner, A. Varykhalov, R. Follath, and S. V. Borisenko, Nature (London) **457**, 569 (2009).
[11] This pocket is named "blade" because the whole structure around the *X* point—*X*-pocket and four blades—reminds one of a propeller.
[12] R. C. Dynes, V. Narayanamurti, and J. P. Garno, Phys. Rev. Lett. **41**, 1509 (1978).
[13] S. Tsuda, T. Yokoya, T. Kiss, Y. Takano, K. Togano, H. Kito, H. Ihara, and S. Shin, Phys. Rev. Lett. **87**, 177006 (2001).
[14] Note that nonsuperconducting part shown in Fig. 5(a) also contains momentum-independent part that should be subtracted.
[15] J. T. Park, D. S. Inosov, Ch. Niedermayer, G. L. Sun, D. Haug, N. B. Christensen, R. Dinnebier, A. V. Boris, A. J. Drew, L. Schulz, T. Shapoval, U. Wolff, V. Neu, X. Yang, C. T. Lin, B. Keimer, and V. Hinkov, arXiv:0811.2224 (unpublished).
[16] T. Goko, A. A. Aczel, E. Baggio-Saitovitch, S. L. Budko, P. C. Canfield, J. P. Carlo, G. F. Chen, W. Z. P. Dai, A. Hamann, W. Hu, H. Kageyama, G. M. Luke, J. L. Luo, B. Nachumi, N. Ni, D. Reznik, D. R. Sanchez-Candela, A. T. Savici, K. J. Sikes, N. L. Wang, C. R. Wiebe, T. J. Williams, T. Yamamoto, W. Yu, and Y. J. Uemura, arXiv:0808.1425 (unpublished).
[17] G. L. Sun, D. L. Sun and C. T. Lin, arXiv:0901.2728 (unpublished).
[18] D. V. Evtushinsky, A. A. Kordyuk, S. V. Borisenko, V. B. Zabolotnyy, M. Knupfer, J. Fink, B. Buchner, A. V. Pan, A. Erb, C. T. Lin, and H. Berger, Phys. Rev. B **74**, 172509 (2006).
[19] I. I. Mazin and M. D. Johannes, Nat. Phys. **5**, 141 (2009).
[20] A. A. Kordyuk, S. V. Borisenko, M. Knupfer, and J. Fink, Phys. Rev. B **67**, 064504 (2003).
[21] Here we can neglect variations in the matrix elements as relevant scales in momentum space are rather small.
[22] Rigorously speaking, we use the following mathematical fact, $\int_{-\infty}^{+\infty}(f_1 \otimes f_2)dx = \int_{-\infty}^{+\infty} f_1 dx \int_{-\infty}^{+\infty} f_2 dx$, which in our case reads $\int A(k,\omega) \otimes R_k dk = \int A(k,\omega)dk \int R_k(k)dk$.
[23] G. D. Mahan, *Many Particle Physics* (Plenum, New York, 1981).
[24] H.-B. Yang, J. D. Rameau, P. D. Johnson, T. Valla, A. Tsvelik, and G. D. Gu, Nature (London) **456**, 77 (2008).
[25] T. Baba, T. Yokoya, S. Tsuda, T. Kiss, T. Shimojima, K. Ishizaka, H. Takeya, K. Hirata, T. Watanabe, M. Nohara, H. Takagi, N. Nakai, K. Machida, T. Togashi, S. Watanabe, X.-Y. Wang, C. T. Chen, and S. Shin, Phys. Rev. Lett. **100**, 017003 (2008).
[26] A. A. Kordyuk, S. V. Borisenko, A. Koitzsch, J. Fink, M. Knupfer, and H. Berger, Phys. Rev. B **71**, 214513 (2005).